

University of Groningen

Gravitational imaging of cold dark matter substructures

Koopmans, L. V. E.

Published in:
Monthly Notices of the Royal Astronomical Society

DOI:
[10.1111/j.1365-2966.2005.09523.x](https://doi.org/10.1111/j.1365-2966.2005.09523.x)

IMPORTANT NOTE: You are advised to consult the publisher's version (publisher's PDF) if you wish to cite from it. Please check the document version below.

Document Version
Publisher's PDF, also known as Version of record

Publication date:
2005

[Link to publication in University of Groningen/UMCG research database](#)

Citation for published version (APA):
Koopmans, L. V. E. (2005). Gravitational imaging of cold dark matter substructures. *Monthly Notices of the Royal Astronomical Society*, 363(4), 1136-1144. <https://doi.org/10.1111/j.1365-2966.2005.09523.x>

Copyright

Other than for strictly personal use, it is not permitted to download or to forward/distribute the text or part of it without the consent of the author(s) and/or copyright holder(s), unless the work is under an open content license (like Creative Commons).

Take-down policy

If you believe that this document breaches copyright please contact us providing details, and we will remove access to the work immediately and investigate your claim.

Downloaded from the University of Groningen/UMCG research database (Pure): <http://www.rug.nl/research/portal>. For technical reasons the number of authors shown on this cover page is limited to 10 maximum.

Gravitational imaging of cold dark matter substructures

L. V. E. Koopmans[★]

Kapteyn Astronomical Institute, PO Box 800, 9700 AV Groningen, the Netherlands

Accepted 2005 August 9. Received 2005 July 25; in original form 2005 January 23

ABSTRACT

We propose the novel method of ‘gravitational imaging’ to detect and quantify luminous and dark matter substructures in gravitational lens galaxies. The method utilizes highly magnified Einstein rings and arcs as sensitive probes of small perturbations in the lens potential (due to the presence of the mass substructure), reconstructing the gravitational lens potential non-parametrically. Numerical simulations show that the implemented algorithm can reconstruct the smooth mass distribution of a typical lens galaxy – exhibiting reasonable signal-to-noise Einstein rings – as well as compact substructure with masses as low as $M_{\text{sub}} \sim 10^{-3} M_{\text{lens}}$, if present. ‘Gravitational imaging’ of pure dark matter substructures around massive galaxies can provide new insight into the standard cold dark matter paradigm, using very different physics than ground-based direct-detection experiments, and probe the hierarchical structure-formation model which predicts that this substructure exists in great abundance.

Key words: gravitational lensing.

1 INTRODUCTION

Arcsecond-scale strong gravitational lens systems (i.e. those with multiple lensed images) provide a wealth of information about cosmology, the lensed source and the lens galaxies themselves and considerable progress has been made in all three fields in the last 25 years (see e.g. Kochanek, Schneider & Wambsganss 2004). However, the accuracy in many applications (e.g. measuring H_0 ; Refsdal 1964) is set by the poor understanding of the mass distribution of the lens potential, limiting at the same time the use of strong lenses as galaxy structure probes (e.g. Kochanek 1991).

It is therefore critical to exploit all available information to constrain the lens potential, for example by including non-lensing data (e.g. stellar dynamics; Koopmans & Treu 2002) – and/or extract all information on the lens potential from extended lensed images. The general problem, however, is how to solve this issue simultaneously for both the structure of the lensed source and the structure of the lens potential (or the lens mass distribution). Information on both are entangled in the complex structure of multiple lensed images.

A significant step forward in disentangling this information and using it to constrain the lens potential, is the use of non-parametric image reconstruction techniques in which the source brightness distribution is reconstructed on an, in some cases adaptive, grid (e.g. Kochanek et al. 1989; Wallington, Kochanek & Koo 1995; Ellithorpe, Kochanek & Hewitt 1996; Wallington, Kochanek & Narayan 1996; Warren & Dye 2003; Treu & Koopmans 2004; Wucknitz 2004; Wucknitz, Biggs & Browne 2004; Wayth et al. 2005; Dye & Warren 2005; Brewer & Lewis 2005). These tech-

niques fully exploit all information contained in the lensed images. The use of smooth¹ parametrized potential models ensures relative ease in the separation of information about the source and the potential, as the degree of flexibility in the potential models is significantly less than in the source model.

To overcome a certain lack of freedom in the parametrized potential/mass models, Saha & Williams (1997) developed a non-parametric mass reconstruction technique. Their implementation, however, only uses constraints from point-like images and the number of free parameters in the mass models often far exceeds the number of genuine constraints. The interpretation of the results must therefore be done statistically (e.g. Williams & Saha 2000). Even so, the method is powerful in exposing the range of mass models (although some might not be physical) for systems with lensed point images only.

Gravitationally lensed images, however, are strongly correlated representations of the same lensed source, whereas the effect of the lens potential on them should be highly uncorrelated on small scales. This allows them to be non-parametrically separated to a very large degree.

To illustrate this point more vividly, suppose that one observes a two- or four-image lens system. Any change in the source structure will show up in all multiple images. Conversely, similar structures in the lensed images most likely arise from structures in the source and not from the unlikely coincidence of nearly identical (small-scale) perturbations in the lens potential that happen to occur exactly in front of all lensed images. In contrast, clear structure in only one, hence not all, of the lensed images is most easily explained by a

[★]E-mail: koopmans@astro.rug.nl

¹ I.e. slowly varying on the scales of the lensed images.

localized perturbation of the lens potential near that particular image. By casting this in likelihood terms, this illustration tells us that correlated structures in the lensed images – even though they could be not excluded to arise from small-scale perturbations in the lens potential in front of all lensed images – is most likely the result of structure in the source. Likewise, uncorrelated structure in the lensed images is most likely the result of small-scale perturbations in the lens potential. This forms the basis of a maximum-likelihood (ML) technique that allows the source and potential information encoded in the multiple lensed images, to be separated. This does not imply, however, that all degeneracies are broken (e.g. the mass-sheet degeneracy; Falco, Gorenstein & Shapiro 1985). It does, however, allow greater freedom in the lens-potential models and the possibility of reconstructing small scale potential perturbations, arising from mass substructure, if present.

In this paper, we have developed this notion further and extensively modify the non-parametric source reconstruction algorithm – as implemented in Treu & Koopmans (2004)² – to allow for a simultaneous non-parametric source and lens-potential reconstruction. This integrates the idea initially suggested by Blandford, Surpi & Kundić (2001) and more recently by Suyu & Blandford (2005), with the semi-linear inversion technique by Warren & Dye (2003) as implemented in Treu & Koopmans (2004) into a single mathematical framework. Through the two-dimensional Poisson equation, the lens potential provides a direct gravitational image of the surface density of the lens galaxy, not affected (or potentially biased) by external shear.

The technique of gravitational imaging allows dark matter substructures in cosmologically distant lens galaxies to be detected, imaged and quantified. Flux-ratio anomalies have already hinted at its existence, either dark or luminous (e.g. Mao & Schneider 1998; Metcalf & Madau 2001; Chiba 2002; Metcalf & Zhao 2002; Dalal & Kochanek 2002; Bradač et al. 2002; Keeton 2003). If indeed these anomalies are caused by perturbations of the underlying smooth lens-galaxy potential, a direct image of the lens-galaxy mass distribution could settle many of the still open questions, such as which mass scale contributes most to flux-ratio anomalies and whether this mass is associated with the lens galaxy (Bradač et al. 2004; Mao et al. 2004; Amara et al. 2005; Metcalf 2005).

Moreover, the unequivocal detection of dark matter substructures around lens galaxies – without any reasonable mass-to-light ratio counterpart in deep high-resolution optical images – would be a direct vindication of the basic cold-dark matter paradigm that predicts that they exist in large numbers (Moore et al. 1999; Klypin et al. 1999). Because substructures are expected to be more prevalent at higher redshifts (e.g. Gao et al. 2004), lens galaxies are excellent probes and gravitational imaging an excellent way to test and quantify the basic assumptions of the dark matter and the hierarchical structure-formation models.

In Section 2, we derive an iterative set of linear equations that can be solved simultaneously for the source structure and the lens potential. We also discuss which form of regularization to use and

how to determine the regularization parameters through ML analysis. In Section 3, we illustrate the method with a simulated Einstein ring. In Section 4, we draw our conclusions.

2 THE METHOD

In this section, before we extend the non-parametric method to include a non-parametric reconstruction of the lens potential, we first discuss the non-parametric reconstruction method for only a pixelized source, but given a smooth parametrized lens-potential model.

2.1 The non-parametric source solution

The non-parametric reconstruction method of a pixelized source is shown schematically in Fig. 1. The figure illustrates how the surface brightness of each image pixel can be represented through a weighted linear superposition of the (unknown) surface brightnesses at four source pixels. Hence, one can represent this as a simple linear equation (see Treu & Koopmans 2002) and because this holds for each of the $M \times N$ images pixels, one obtains a set of $M \times N$ coupled³ linear equations. This set of equations is constrained by the $M \times N$ observed surface brightness values (i.e. \mathbf{d}) and has $K \times L$ free parameters (i.e. \mathbf{s} ; the unknown surface brightness values on the source grid).

As was shown in Koopmans & Treu (2002) and also in Warren & Dye (2003), the pixelized lensed image (with the lens-galaxy subtracted and blurring included) can then be expressed as the set of linear equations

$$\mathbf{BL}(\psi)\mathbf{s} = \mathbf{d}, \quad (1)$$

where $\mathbf{L}(\psi)$ and \mathbf{B} are the lensing and (also linear) blurring operators, respectively, and ψ is the lens potential which for simplicity here also represents the set of unknown lens-potential parameters. Each row of the lensing operator (a sparse matrix) only contains the four bi-linear interpolation weights, placed at the columns that correspond to the four source pixels that enclose the associated source position (Fig. 1; see Treu & Koopmans 2004 for details).

The set of equations (1) is in general ill-posed (i.e. under-constrained and/or noisy data) and can not be solved through $\mathbf{s} = [\mathbf{BL}(\psi)]^{-1}\mathbf{d}$. Instead, there exist well-known regularized inversion techniques that minimize the quadratic penalty function

$$G(\mathbf{s}, \psi) = \|\mathbf{M}\mathbf{s} - \mathbf{d}\|_2^2 + \sum_i \lambda_i \|\mathbf{H}_i\mathbf{s}\|_2^2, \quad (2)$$

by varying \mathbf{s} [we define $\mathbf{M} \equiv \mathbf{BL}(\psi)$]. In addition, \mathbf{H}_i are regularization matrices and λ_i are the corresponding regularization parameters, both of which we discuss in more detail below (see also Press et al. 1992 for a clear discussion about regularization methods). The first term in the penalty function $G(\mathbf{s}, \psi)$ is proportional to the total χ^2 for a given solution \mathbf{s} and as such quantifies how well the model matches the data. The second terms can regularize the ‘smoothness’ of the solution by adding a positive quadratic penalty term, whose argument depends linearly on the source solution, i.e. through $\mathbf{H}_i\mathbf{s}$, which for example could give its n th order derivative. The quadratic nature of the regularization term ensures that the minimum- G solution can be found by solving a linear set of equations (this is not the case for maximum-entropy or ML regularization terms). The

² We note that the implementation of the semi-linear inversion technique in Warren & Dye (2003) is similar to that in Treu & Koopmans (2004) and does not require the inversion of the lens equation as previously suggested. Both implementations, however, differ in their determination of the lens and blurring operators (Dye, private communications). Regularization is done through a quadratic term added to the χ^2 penalty function, which ensures linearity of the set of equations whose solution minimizes the penalty function (ML or entropy terms are not quadratic and lead to a non-linear set of equations that need to be solved iteratively).

³ The brightnesses of multiple image pixels can depend on the brightness of a single source pixel (see the caption of Fig. 1).

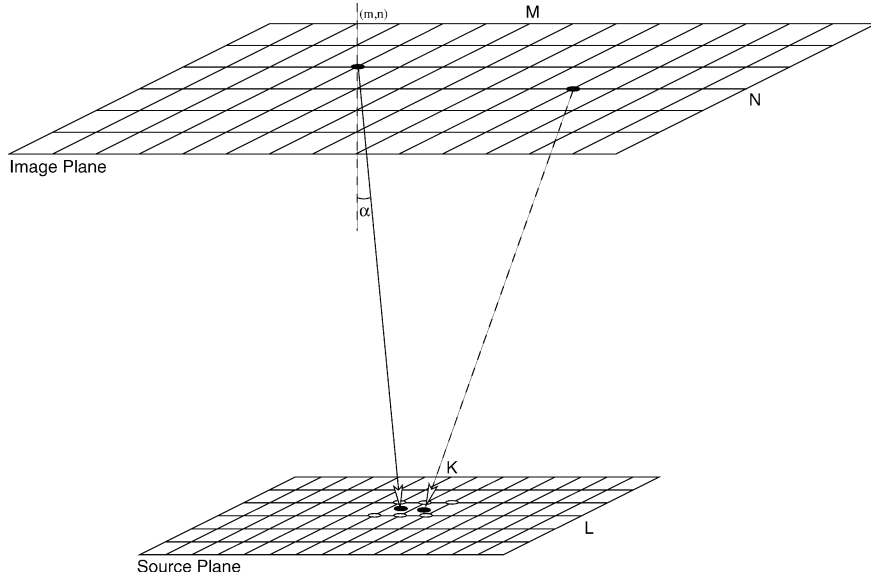


Figure 1. A schematic overview of the method of non-linear image (i.e. source) reconstruction, as implemented by Treu & Koopmans (2004) and in this paper. In the absence of blurring or averaging inside the pixels, the position (\mathbf{x}) of each pixel (m, n) in the image plane corresponds to a position in the source plane (\mathbf{y}), through the lens equation $\mathbf{y} = \mathbf{x} - \alpha(\mathbf{x})$. The surface brightnesses at these corresponding points – conserved through lensing – are the same. Because the source brightness distribution is reconstructed on a fixed grid, the surface brightness at \mathbf{y} , i.e. $\Sigma(\mathbf{y}) = \Sigma(\mathbf{x})$, is represented by a linear superposition of the surface brightnesses at the four pixels that enclose \mathbf{y} (open circles). The weights for each of these source pixels are the bilinear interpolation weights, whose sum add to unity to conserve flux (higher-order interpolation is also possible; see Treu & Koopmans 2004). This way – because of the multiple nature of the lensed images – there can be more than one constraint on a single source pixel (depending on its size and the number of multiple images). In addition, because there are multiple solutions of four weighted brightnesses adding to the observed brightness at \mathbf{x} , regularization is often required to ensure a relatively smooth and more physical source brightness distribution for lower S/N ratio data (see text).

quadratic nature of the regularization term dramatically reduces the time to numerically find the best source solution and ensures that the global minimum of G is found (given a fixed ψ).

By setting the derivative $\partial G(s, \psi)/\partial s = 0$, a bit of linear algebra then leads to the required set of equations

$$\left[\mathbf{M}^T \mathbf{M} + \sum_i \lambda_i \mathbf{H}_i^T \mathbf{H}_i \right] \mathbf{s} = \mathbf{M}^T \mathbf{d}, \quad (3)$$

whose solution for \mathbf{s} minimizes $G(s, \psi)$, by construction, for a fixed lens potential ψ . In an outer non-linear optimization loop (see Warren & Dye 2003) one then varies the free parameters of ψ to find the global minimum of the joint penalty function, $G(s, \psi)$, resulting in an optimized non-parametric source model and an optimized set of parameter values for the lens potential.

In this way, one makes full use of all the information in the lensed images to constrain the parametrized potential model ψ , without any strong assumptions about the structure of the source. However, there are several questions that arise, as follows.

- (i) Does the parametrized potential model ψ have enough freedom to describe the true lens potential?
- (ii) Which form for the regularization matrices, \mathbf{H}_i , should be used?
- (iii) What should be the values of the regularization parameters λ_i in the penalty function G ?

To (partly) address these questions, we derive in Section 2.2 a new set of linear equations, whose min- G solution gives the pixelized source structure and simultaneously a linear pixelized correction ($\delta\psi$) to the initial model of the lens potential. By solving this new set of equations and correcting the potential model iteratively, one

minimizes the penalty function to find a non-parametric and non-linear solution for both the source structure and the lens potential.

We choose to pixelize and solve for the lens potential, in contrast to, for example, Saha & Williams (1997) who solve this for a pixelized mass distribution. Both are related through the two-dimensional Poisson equation. However, because all properties of the lens system can be derived solely from the local lens potential (through its zero-, first- and second-order derivatives), no assumptions have to be made about what happens outside the region where we have lensing information (i.e. the lensed images). On the other hand, if one chooses to use a pixelized mass distribution, one needs to make some a priori assumptions about the mass distribution outside the grid (e.g. no mass), because mass outside the grid still contributes to the lens potential inside the grid. If wrong assumptions are made, for example one assumes there is no potential arising from external shear [i.e. $\psi_{\text{sh}}(\mathbf{x}) = 0$] whereas in fact there is, one can severely bias the resulting solution for the pixelized mass distribution, because the contribution from shear must then somehow be mimicked by the mass distribution inside the grid.

In the case of a pixelized potential model, however, the lens potential due to external mass (i.e. from outside the grid) would be reconstructed without a problem, just like that arising from mass inside the grid. The Poisson equation, furthermore, only gives the mass distribution inside the grid, not affected by, for example, external shear (because $\nabla^2 \psi_{\text{sh}}(\mathbf{x}) = 0$) or any mass external to the grid. The reconstructed mass distribution can therefore never be biased by assumptions about the mass distribution outside the grid. We regard the latter as a great advantage over the use of a pixelized mass distribution.

A second advantage of using the lens potential over the lens mass distribution is increased numerical speed in the optimization process. In case a mass distribution is used, the lens potential still needs

to be calculated through a convolution. This is a significant numerical burden, whereas all lens properties can simply and quickly be derived from a lens potential through its n th order derivatives ($n = 0, 1$ or 2).

Despite these advantages, the use of a pixelized mass distribution as a means of retaining a positive surface density. However, when we regularize the potential model by minimizing the norm of its n th order derivative, we regularize the mass density in its $(n - 2)$ th order derivative (because of the second-order derivative in the Poisson equation). Because we start with a smooth positive-density mass model and only make a relative small potential correction, the regularization can thus ensure that the surface density of the mass model remains positive, even though we reconstruct the lens potential (see also Section 2.3.1).

The second and third questions, stated above, are of more general interest in many similar (image-reconstruction) problems and are addressed in Sections 2.3 and 2.4, within the context of the problem at hand.

2.2 The non-parametric source and potential solutions

To find a linear correction to, say, a parametrized potential model (e.g. found as described in Section 2.1) we assume that the potential ψ is also pixelized⁴ (i.e. ψ are the pixel values). We note that the number and size of the pixels for the potential grid need not be the same as for the image grid.

Given the previously found best-fitting source model s_p and potential-model ψ_p , one can then subtract the best-fitting lens model from the data and obtain a residual image

$$\delta d = d - \mathbf{M}(\psi_p) s_p. \quad (4)$$

If $\|\delta d / \sigma_d\|^2 \gg (MN)$, where σ_d^2 is the variance per the image pixel, either the source or the potential model is not correct, or both. We can then assume that a potential correction ($\delta\psi$) exists, for which in the first order we have

$$d - \mathbf{M}(\psi_p + \delta\psi) s_p \rightarrow 0. \quad (5)$$

It is our task to find $\delta\psi$ and with it correct the previously best-fitting potential model $\psi_p + \delta\psi \rightarrow \psi$. With the previous source solution, s_p , this can to the first-order also be written as a new set of linear equations (Appendix A)

$$\delta d = -\mathbf{B}\mathbf{D}_s(s_p)\mathbf{D}_\psi\delta\psi, \quad (6)$$

where $\mathbf{D}_s(s_p)$ is a sparse matrix whose entries depend on the gradient of the previously best source model and \mathbf{D}_ψ is a matrix that determines the gradient of $\delta\psi$. Note also that the image blurring is accounted for (see Koopmans & Treu 2004). Combining equation (6) with equation (4), one finds

$$\mathbf{B}[\mathbf{L}(\psi_p)s - \mathbf{D}_s(s_p)\mathbf{D}_\psi\delta\psi] = d. \quad (7)$$

If we further introduce the block matrix

$$\mathbf{L}_c(\psi_p, s_p) \equiv (\mathbf{L}(\psi_p) | -\mathbf{D}_s(s_p)\mathbf{D}_\psi) \quad (8)$$

and the block vector

$$\mathbf{r} \equiv \begin{pmatrix} s \\ \delta\psi \end{pmatrix}, \quad (9)$$

⁴ Because we determine a correction to the initial potential model – which itself might be parametrized – we in principle only need to pixelize the potential correction and not the initial ψ . The result, however, is the same.

the final linear set of equations becomes

$$\mathbf{B}\mathbf{L}_c(\psi_p, s_p)\mathbf{r} \equiv \mathbf{M}_c\mathbf{r} = d. \quad (10)$$

The structure of this equation is the same to that of equation (1) and can thus be solved as before. We note that because the first term of equation (7) depends only on ψ_p and s , whereas the second terms depends only on $\delta\psi$ and s_p , they are decoupled sets of equations that could be solved independently.

How can the correction in equation (6) be interpreted? This is most easily seen when writing the equation in its continuous form $\delta d(\mathbf{x}) = -\nabla_y s(\mathbf{y}) \cdot \nabla_x \delta\psi(\mathbf{x})$ as shown in Appendix A. Because $\mathbf{y} = \mathbf{x} - \nabla\psi$ and $\delta\mathbf{y} = -\nabla\delta\psi$, what equation (6) tells us is that to the first order the deviation of $\delta d(\mathbf{x})$ from zero can be compensated exactly by Taylor expanding $s(\mathbf{y})$ to the first order around \mathbf{y} and then changing the deflection angle slightly by $\delta\mathbf{y}$ to point to that part of the source, close to \mathbf{y} , that has the same surface brightness as that seen at the image position \mathbf{x} . The trick is to find the solution $\delta\psi(\mathbf{x})$ such that $\delta d(\mathbf{x}) \rightarrow 0$ for all \mathbf{x} . This is what has been done above, by linearizing the equations and writing the result in matrix/vector notation.

2.3 The regularization matrix

Because s and $\delta\psi$ are independent, they require their own regularization parameters. Consequently, the regularization matrix needs to be modified somewhat

$$\mathbf{R} \equiv \begin{pmatrix} \sum_j \lambda_{s,j} \mathbf{H}_{s,j}^T \mathbf{H}_{s,j} & 0 \\ 0 & \sum_j \lambda_{\delta\psi,j} \mathbf{H}_{\delta\psi,j}^T \mathbf{H}_{\delta\psi,j} \end{pmatrix}. \quad (11)$$

The set of equations, whose solution minimizes the penalty function, then becomes

$$(\mathbf{M}_c^T \mathbf{M}_c + \mathbf{R}) \mathbf{r} = \mathbf{M}_c^T d. \quad (12)$$

Hence, by iteratively solving equation (12) and correcting the lens potential at each iteration, one finds the source and potential structure that minimize G without strong assumptions about either. This equation is the equivalent of equation (3).

2.3.1 Regularizing with higher-order derivative operators

The form of the regularization matrices is not a priori determined. But as ‘smoothness’ is often a criterion for how well the reconstruction has been done, most often derivative operators are used for the regularization matrices (see Press et al. 1992 for some examples); the zeroth-order derivative being the identity matrix. Their mathematical structure is also well understood of all forms (see Neumaier 1998 for a complete analysis).

We use different derivative orders for the source and the potential regularization. We find that the zeroth-order derivative, $\mathbf{H} = \mathbf{I}$, gives poor source reconstruction in the majority of cases, especially if the signal-to-noise (S/N) ratio of the data is low (see Treu & Koopmans 2004 for a discussion) and worse for the potential reconstruction, that requires smoothness in a very high order (see the following sections). One solution is to resort to *multiscale* pixels in the source plane (Dye & Warren 2005), which is an implicit form of adaptive regularization. But it is hard to require smoothness (or continuity) in the solutions and their derivatives.

For this reason, a much better choice of regularization for *single-scale* pixels, is the use of higher-order derivative operators. In those

cases neighbouring pixels are ‘connected’, resulting in considerably improved solutions.⁵

It is found that regularization with a single second-order derivative operator (i.e. minimizing curvature) is often sufficient to reconstruct the source. To require the convergence (i.e. surface density) of the lens to be smooth, the potential regularization requires at least a single fourth-order derivative operator.⁶ As $\delta\kappa/\kappa \ll 1$ and $\delta\kappa$ are smooth for any good starting model, one ensures in general positive convergence solutions.

2.4 The regularization-parameter values

Having chosen appropriate regularization matrices, the next question is which level of regularization is appropriate.

(i) The ‘subjective’ way of choosing their numerical values is through a careful analysis of simulated lens systems that closely resemble the real lens system. The regularization-parameters values are then chosen such that the input models are best recovered. Because the real system resembles the simulated system, one assumes that the obtained value for the regularization parameter also gives an unbiased reconstruction of the source and potential of the real system.

(ii) The ‘objective’ way is to have the data itself determine the regularization-parameter values. Intuitively, one might think that the probability distribution of pixel values of the difference between the observed system and the model should be that of ‘noise’ with zero mean and show no residual structures. How can in that case, the numerical values of $\lambda_{s/\delta\psi,j}$ be determined?

As is often the case in CCD images, if the noise is approximately Gaussian distributed, this can be expressed for a fixed ψ , as the maximization of the likelihood

$$\mathcal{L} = \frac{1}{(2\pi)^{NM/2} \sqrt{\det(\sigma_d^2 \mathbf{I})}} \exp\left[-(\mathbf{d} - \mathbf{M}\tilde{s})^T(\mathbf{d} - \mathbf{M}\tilde{s}) / (2\sigma_d^2)\right], \quad (13)$$

with σ_d^2 being the variance of the image pixels, assuming that the covariance between different pixels is zero and \tilde{s} being the solution from equation (3). What this equation means is that the ML value of λ should, as closely as possible, result in a zero-mean Gaussian residual image $\delta\mathbf{d}$. As an illustration, if λ (encoded in \tilde{s}) is too small, the model will fit the noise, resulting in a ‘flat’ residual distribution function (i.e. the lowest noise values becomes part of the model and consequently do not show up in the residual image). On the other hand, if λ is too large, the residual image will show coherence non-Gaussian structures that could not be fitted because of over-regularization. In both cases, the residuals deviate from Gaussian, resulting in a low likelihood for the model.

Using the estimate of \tilde{s} from equation (3), it has been shown shown by Wahba (1985; see also Neumaier 1998) that the ML value of the regularization parameter for the source can then be found by maximizing the likelihood function

$$\mathcal{L} = \log(\|\mathbf{d}\|_2^2 - \|\mathbf{u}\|_2^2) - \log(\lambda) + \frac{2}{n} \log \det(\mathbf{C}), \quad (14)$$

where $\mathbf{C}\mathbf{C}^T = \mathbf{M}^T\mathbf{M} + \lambda\mathbf{H}^T\mathbf{H}$ is obtained through a Cholesky decomposition, \mathbf{u} is found by solving $\mathbf{C}\mathbf{u} = \mathbf{M}^T\mathbf{d}$ and $n = KL$

⁵ Of course, any choice of regularization is *ad hoc* at some level. Only by testing the different choices can one assess whether regularization gives a (physically) acceptable solution.

⁶ The convergence is derived from the potential using second-order derivatives in the Poisson equation.

is the number of source pixels. The result is independent from the variance σ_d^2 , which therefore does not have to be explicitly known a priori. The ML solution of the source is obtained by solving $\mathbf{C}^T\mathbf{s} = \mathbf{u}$. Hence equation (14) is the equivalent of equation (13), but now explicitly expressed with λ and in such a way that it is easy to solve numerically through a Cholesky decomposition that also gives the solution for s without much additional effort (i.e. through a fast back-substitution, because \mathbf{C} is a diagonal matrix).

As we solve iteratively for the lens potential, it is found that the value of the regularization for the potential is almost irrelevant if chosen to be large enough (it just takes longer to converge for stronger regularization). Furthermore, as the solutions of s and ψ are decoupled in the set of linear equations, as we discussed above, determining the value of λ for the source separately from the potential is mathematically correct.

3 GRAVITATIONAL IMAGING OF GALAXY (SUB)STRUCTURE

Having introduced the methodology above, we refer to appendix B for an outline an iterative algorithm of the method. Although it is not necessarily the only or most optimal implementation, it is relatively easy to implement and robust. To test the algorithm, we performed a simulation of an artificial Einstein-ring and subsequently reconstruct the source and lens potential.

In Section 3.1, we first describe the simulated lens system. The source is chosen to be a double structure, consisting of two elliptical galaxies. Similarly, the lens is a smooth elliptical mass distribution plus an additional low-mass substructure. The aim of this simulation is to show that the method/algorithm is capable of reconstructing both the source structure and the small-scale mass distribution (i.e. the mass substructure) on the lens galaxy.

3.1 Artificial Einstein-ring lens system

The components of the lens system are as follows.

(i) Lens mass model. The lens mass model consists of a single Singular Isothermal Ellipsoid (SIE) lens (Kormann, Schneider & Bartelmann 1994) with a lens strength of $b = 0.9$ arcsec, a position angle (PA) of $\theta = 45^\circ$, an axial ratio of $f = (b/a)_\kappa = 0.8$ and centred at (0.0, 0.0) arcsec. The mass model also includes a dwarf satellite represented by a SIS with $b = 0.045$ arcsec at $(-0.9, -0.4)$ arcsec (placed on the Einstein ring). As typical lens galaxies with these image separations have $M_E \sim 10^{11} M_\odot$ inside their Einstein radius, this particular substructure has a mass of $M_E \sim 10^8 M_\odot$.

(ii) Source brightness model. To show that complexity in the source and lens-potential models can be disentangled, the source consist of two components. (1) A subcomponent with an elliptical exponential brightness profile with 0.1-arcsec scalelength, a central surface brightness of 100 arcsec^{-2} (arbitrary units), an axial ratio of 0.64, a PA = 113° and centred at $(-0.05, 0.05)$ arcsec. (2) A subcomponent with an exponential brightness profile of 0.1-arcsec scalelength, a central surface brightness of 50 arcsec^{-2} , centred at $(-0.40, 0.25)$ arcsec. The source is pixelized on a $1.0 \times 1.0 \text{ arcsec}^2$ grid of 30×30 pixel.

(iii) Simulated lensed images. The lensed image is calculated on a $3 \times 3 \text{ arcsec}^2$ grid of 60×60 pixel and blurred by an artificial *HST*-ACS F814W point spread function (PSF). Gaussian noise with $\sigma = 1$ is added to the resulting blurred image. The simulated system and reconstructed source model are shown Fig. 2.

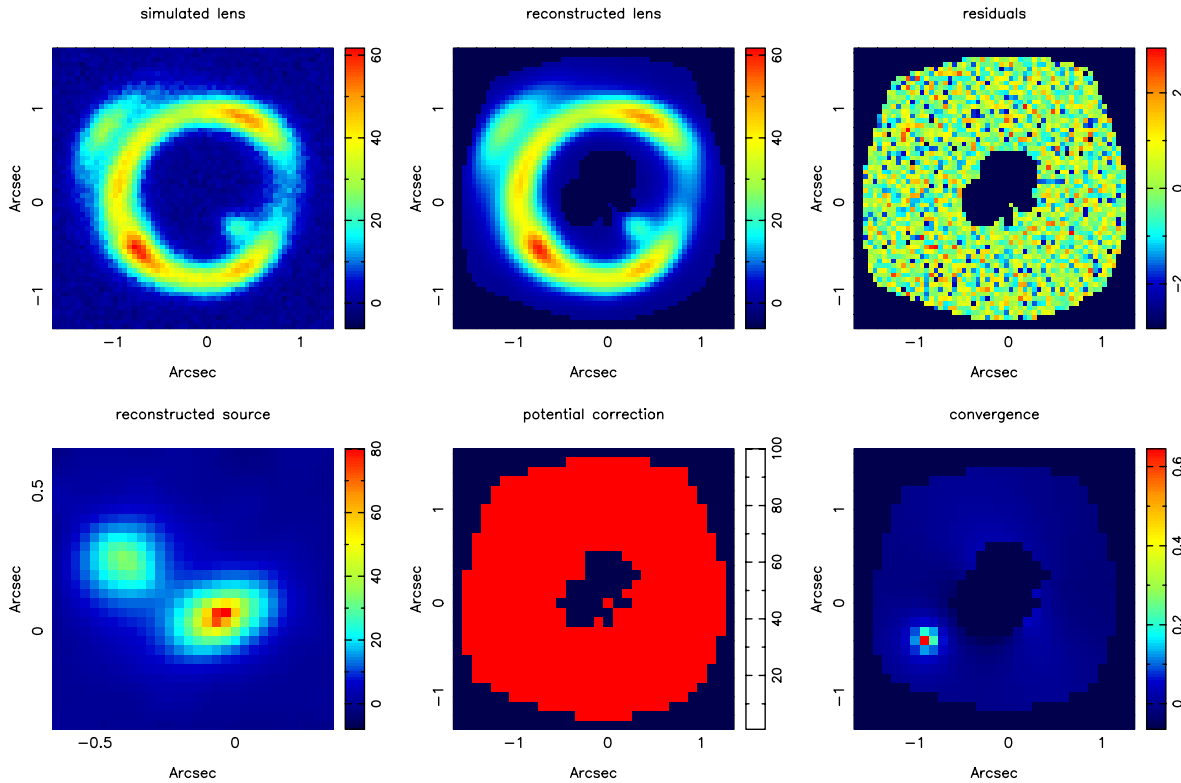


Figure 2. Reconstruction of the source and lens-potential correction using the true mass model. Top row: a simulated Einstein–Ring lens system (see text) (left). The best reconstruction (middle) and residuals (right). Bottom row: the reconstructed source (left). The correction to the lens potential, set to zero for this model (middle), and the total convergence minus a best-fitting SIE mass model (right). The shape of the reconstructed region is determined by the projection of the rectangular source plane on to the image plane. This results in a hole in the centre of the reconstruction, because the source plane (in this case) maps on to a closed annulus. Outside the annulus, image-plane pixels map outside the source-plane grid.

3.2 The non-parametric source and lens-potential reconstruction

We perform two reconstructions. The first is a test-run and reconstructs only the source structure, assuming that we have perfect knowledge of the true lens mass model. This is not a realistic situation, but it shows that the method properly recovers the input source model without significant residuals. The potential grid is defined on a $3 \text{ arcsec} \times 3 \text{ arcsec}$ grid of 30×30 pixel, sufficient to capture any (sub)structure in the lens potential. The result is shown in Fig. 1. The input source and Einstein ring are nicely reconstructed and the residuals are not significant ($\chi^2/\text{NDF} = 0.96$).

The second run should represent a more realistic situation. As would be done with an observed lens system, we find the source and lens-potential model in a number of distinct steps. (1) First, we fit a single SIE mass model to the four image centroids; the resulting best-fitting parameters are $b = 0.85 \text{ arcsec}$, a PA of $\theta = 47^\circ$, an axial ratio of $f = (b/a)_\kappa = 0.84$). The residuals have $\chi^2/\text{NDF} = 29.4$, hence the model is dramatically far from the true mass model (see Fig. 3). Although statistically a very poor model, we can use this as the initial starting model for the non-parametric reconstruction. (2) We non-parametrically reconstruct the source and the lens-potential correction, with a regularization parameter for the source ($\lambda_s = 3.0$; which is clearly too large) and the potential ($\lambda_{\delta\psi} = 10^9$), respectively. We lower the regularization parameters of the potential by 0.1 of its previous value each iteration and iterate ~ 60 times, until convergence (~ 30 min on a 3-GHz laptop). (3) Using this solution, which is an extreme improvement ($\chi^2/\text{NDF} = 1.19$), we use the ML technique (Section 2.4) to determine the value of the source

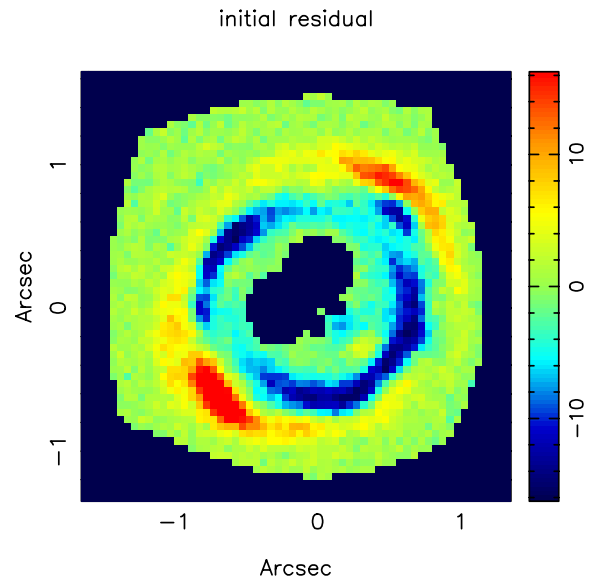


Figure 3. The residuals of the data minus the ‘best’ reconstruction, assuming a SIE mass model fitted to the image centroids only. Note the difference with the final residuals in Fig. 4.

regularization parameter, $\lambda_s^{\text{ML}} = 0.4$. (4) We rerun the simulation with the new value of the regularization parameter. We note that the precise value of λ_s in the second run is nearly independent from its value in the first run, justifying this approach.

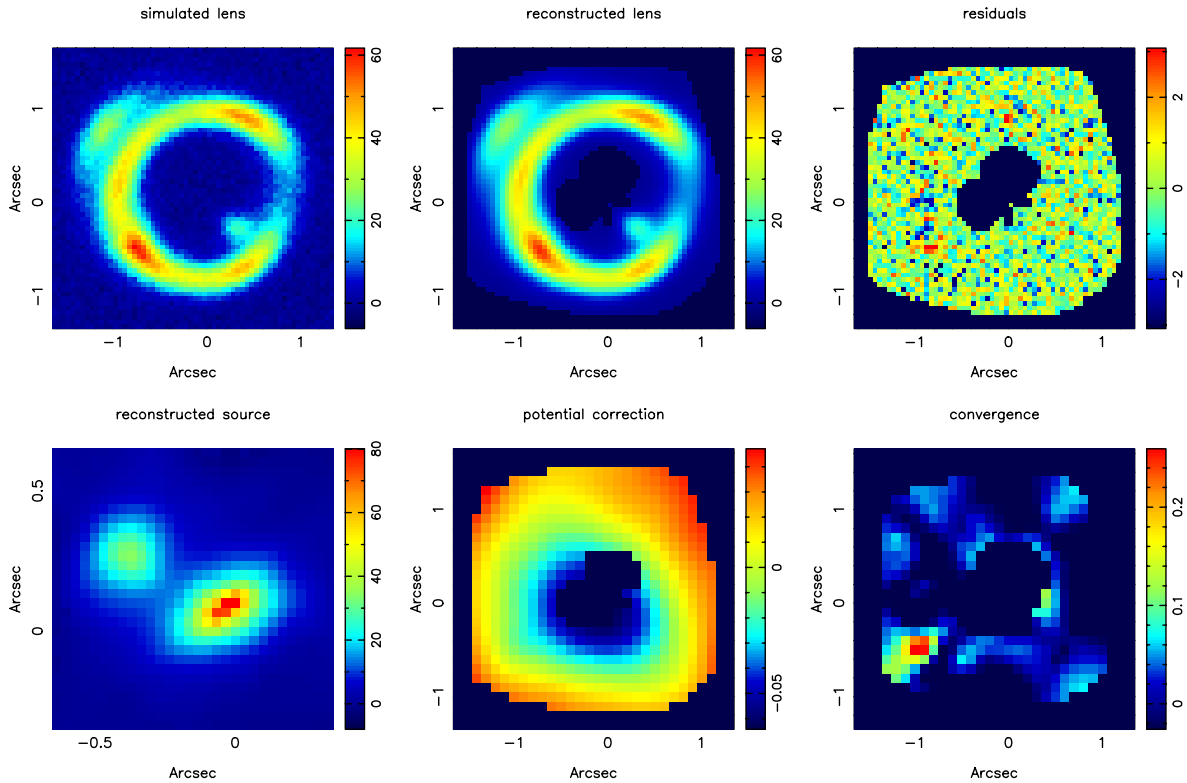


Figure 4. Reconstruction of the source and lens-potential correction using a best-fitting single SIE mass model as a starting model. Top row: a simulated Einstein-Ring lens system (see text) (left). The best reconstruction (middle) and residual images (right). Bottom row: the reconstructed source (left). The correction to the lens potential (middle) and the lens convergence minus a best-fitting SIE mass model (right).

The best model has $\chi^2/\text{NDF} = 1.05$ and is shown in Fig. 4, a dramatic improvement over the best-fitting single SIE mass model. We subtract a best-fitting single SIE mass model (fitted to the total convergence; see lower-right panel) to highlight any lens substructures. The small mass perturbation is indeed recovered near the correct position and with good dynamic range, compared with the residuals in the convergence field. We note that regularization smooths the structure of the small mass component, which is unavoidable. However, within a 0.7×0.7 arcsec² aperture centred on the substructure (approximately the region of positive convergence after the smooth model was subtracted), we recover the original mass of the substructure to within 12 per cent. This shows that one can not only detect, but also quantify its mass.

We note that the final solution has a positive convergence everywhere inside the grid. In Figs 2 and 4 only the convergence is shown after subtracting a smooth SIE model, hence the residual from this could be negative (opposed to the total convergence).

Although we only presented a single simulation in this paper, we find that the algorithm can also reconstruct both the source and the lens potential in more complex and lower S/N ratio cases. A more thorough analysis of the method, its errors and degeneracies, however, is planned. It should include blind tests on N -body simulated lens systems and the use of more realistic source structures.

4 CONCLUSIONS

A new non-parametric source and lens-potential reconstruction method has been presented and implemented. The method has been used on gravitational image substructure in an artificial (but rea-

sonably realistic) lens system, recovering the position and enclosed mass of the substructure, as well as the structure of the lensed source. We also conclude that the method can disentangle structure in the source and lens potential, without strong assumptions about either.

Further improvements, however, are still required as follows. (i) Determination of the full covariance matrix to determine the errors and correlations between the source brightness pixels and potential-correction pixels. (ii) The use of a Markov-Chain Monte Carlo technique to determine the correct (non-linear) errors for each of the source and potential pixel values. This provides a way of estimating errors in real lens systems where Monte Carlo simulations are not feasible. (iii) Testing multiscale pixel schemes (Dye & Warren 2005) against single-scale pixel schemes with adaptive regularization. Due to severe computational limits, however, we have not yet implemented these.

Having demonstrated its feasibility, gravitational imaging can serve as a new tool to discover and quantify the level and evolution of the (dark matter) substructure in the haloes around galaxies at cosmological distances. Through it, the cold dark matter paradigm and the hierarchical structure-formation models can be tested.

ACKNOWLEDGMENTS

The author would like to thank Roger Blandford, Maruša Bradač, Simon Dye, Chris Fassnacht, Phil Marshall, Sherry Suyu, Peter Schneider, Tommaso Treu and Saleem Zaroubi for useful discussions. The author also thanks the referee, Steve Warren, for very helpful comments and suggestions that further improved the presentation and clarity of the paper.

REFERENCES

- Amara A., Metcalf R. B., Cox T. J., Ostriker J. P., 2005, MNRAS, submitted (astro-ph/0411587)
- Blandford R., Surpi G., Kundić T., 2001, in Brainerd T. G., Kochanek C. S., eds, ASP Conf. Ser. Vol. 237, Gravitational Lensing: Recent Progress and Future Goals. Astron. Soc. Pac., San Francisco, p. 65
- Bradač M., Schneider P., Steinmetz M., Lombardi M., King L. J., Porcas R., 2002, A&A, 388, 373
- Bradač M., Schneider P., Lombardi M., Steinmetz M., Koopmans L. V. E., Navarro J. F., 2004, A&A, 423, 797
- Brewer B. J., Lewis G. F., 2005, PASA, 22, 128
- Chiba M., 2002, ApJ, 565, 17
- Dalal N., Kochanek C. S., 2002, ApJ, 572, 25
- Dye S., Warren S., 2005, ApJ, 623, 31
- Ellithorpe J. D., Kochanek C. S., Hewitt J. N., 1996, ApJ, 464, 556
- Falco E. E., Gorenstein M. V., Shapiro I. I., 1985, ApJ, 289, L1
- Gao L., White S. D. M., Jenkins A., Stoehr F., Springel V., 2004, MNRAS, 355, 819
- Keeton C. R., 2003, ApJ, 584, 664
- Klypin A., Kravtsov A. V., Valenzuela O., Prada F., 1999, ApJ, 522, 82
- Kochanek C. S., 1991, ApJ, 373, 354
- Kochanek C. S., Blandford R. D., Lawrence C. R., Narayan R., 1989, MNRAS, 238, 43
- Kochanek C. S., Schneider P., Wambsgans J., 2004, in Meylan G., Jetzer P., North P., eds, Proc. 33rd Saas-Fee Advanced Course, Part 2 of Gravitational Lensing: Strong, Weak & Micro. Springer-Verlag, Berlin
- Koopmans L. V. E., 2004, in Dettmar R., Klein U., Salucci P., eds, Baryons in Dark Matter Halos. Proceedings of Science, http://pos.sissa.it/archive/conferences/014/066/BDMH2004_066.pdf
- Koopmans L. V. E., Treu T., 2002, ApJ, 568, L5
- Kormann R., Schneider P., Bartelmann M., 1994, A&A, 284, 285
- Mao S., Schneider P., 1998, MNRAS, 295, 587
- Mao S., Jing Y., Ostriker J. P., Weller J., 2004, ApJ, 604, L5
- Metcalf R. B., 2005, ApJ, 629, 673
- Metcalf R. B., Madau P., 2001, ApJ, 563, 9
- Metcalf R. B., Zhao H., 2002, ApJ, 567, L5
- Moore B., Ghigna S., Governato F., Lake G., Quinn T., Stadel J., Tozzi P., 1999, ApJ, 524, L19
- Neumaier A., 1998, SIAM Rev., 40, 636
- Press W. H., Teukolsky S. A., Vetterling W. T., Flannery B. P., 1992, Numerical Recipes in C. Cambridge Univ. Press, Cambridge
- RRefsdal S., 1964, MNRAS, 128, 307
- Saha P., Williams L. L. R., 1997, MNRAS, 292, 148
- Schneider P., Ehlers J., Falco E. E., 1992, Gravitational Lenses. Springer Verlag, Berlin
- Suyu S. H., Blandford R. D., 2005, MNRAS, submitted (astro-ph/0506629)
- Treu T., Koopmans L. V. E., 2004, ApJ, 611, 739
- Wahba G., 1985, Ann. Stat., 13, 1378
- Wallington S., Kochanek C. S., Koo D. C., 1995, ApJ, 441, 58
- Wallington S., Kochanek C. S., Narayan R., 1996, ApJ, 465, 64
- Warren S. J., Dye S., 2003, ApJ, 590, 673
- Wayth R. B., Warren S. J., Lewis G. F., Hewett P. C., 2005, MNRAS, 360, 1333
- Williams L. L. R., Saha P., 2000, AJ, 119, 439
- Wucknitz O., 2004, MNRAS, 349, 1
- Wucknitz O., Biggs A. D., Browne I. W. A., 2004, MNRAS, 349, 14

APPENDIX A: LINEAR CORRECTION OF THE LENS POTENTIAL

Given the best-fitting solution to equation (3) for both the potential ψ and source s , one can determine the residual vector

$$\delta \mathbf{d} = \mathbf{d} - \mathbf{M}(\psi) \mathbf{s}. \quad (\text{A1})$$

Hence one subtracts the best lensed source model (blurred with the PSF) from the data. Suppose further that any significant residuals are

due to deviations of ψ from the true potential (this can not strictly be true, because s must also be slightly wrong if ψ is slightly wrong). The question arises which correction to the potential, $\delta\psi$, we have to apply such that, *after the correction*, the residual vector becomes

$$\delta \mathbf{d} = \mathbf{d} - \mathbf{M}(\psi + \delta\psi) \mathbf{s} \approx \mathbf{0}. \quad (\text{A2})$$

This can be derived as follows, for now regarding the image, the source and the potential as scalar functions $d(\mathbf{x})$, $s(\mathbf{x})$ and $\psi(\mathbf{x})$, respectively, and neglecting the PSF. From a simple linear expansion of the lens equation $\mathbf{y} = \mathbf{x} - \nabla_x \psi(\mathbf{x})$ (e.g. Schneider, Ehlers & Falco 1992) it then follows that

$$\mathbf{y} + \delta \mathbf{y} = \mathbf{x} - \nabla_x (\psi(\mathbf{x}) + \delta\psi(\mathbf{x})) \quad (\text{A3})$$

or simply (for a fixed position \mathbf{x})

$$\delta \mathbf{y} = -\nabla_x \delta\psi(\mathbf{x}). \quad (\text{A4})$$

Hence a change in the source position is related to a change in the gradient of the lens potential. By adding a correction, $\delta\psi(\mathbf{x})$, to the lens potential we can ‘move around’ rays of light hitting the source plane. Thus, our task is to find that correction to the potential $\delta\psi(\mathbf{x})$, that obeys the following relation: $s(\mathbf{y} + \delta \mathbf{y}) - s(\mathbf{y}) = \delta d(\mathbf{x})$ [i.e. the brightness of the lensed image at \mathbf{x} equals the brightness of the source at position $\mathbf{x} - \nabla_x (\psi(\mathbf{x}) + \delta\psi(\mathbf{x}))$]. The residual field is then to first order

$$\delta d(\mathbf{x}) = s(\mathbf{y} + \delta \mathbf{y}) - s(\mathbf{y}) \approx \nabla_y s(\mathbf{y}) \cdot \delta \mathbf{y}. \quad (\text{A5})$$

Combining equations (A4) and (A5), one finds

$$\delta d(\mathbf{x}) \approx -\nabla_y s(\mathbf{y}) \cdot \nabla_x \delta\psi(\mathbf{x}), \quad (\text{A6})$$

to first order. This has previously been derived by Blandford et al. (2001). The next step is now to derive the equivalent equation for $\delta \mathbf{d}$ in equation (4). First, we assume that the potential grid has $P \times Q$ pixels (P columns and Q rows) with $p = 1 \dots P$ and $q = 1 \dots Q$. In addition, the potential values are ψ_h with $h = p + (q - 1)P$ and $h = 1 \dots PQ$. The source and data grids are defined and described in Treu & Koopmans (2004). We can now derive equation (4). First, we define

$$\mathbf{D}_s(s_p) = \begin{pmatrix} \dots & \dots & \dots & \dots & \dots \\ \dots & \frac{\partial s_h}{\partial y_1} & \frac{\partial s_h}{\partial y_2} & \dots & \dots \\ \dots & \dots & \dots & \frac{\partial s_{h+1}}{\partial y_1} & \frac{\partial s_{h+1}}{\partial y_2} & \dots \\ \dots & \dots & \dots & \dots & \dots & \dots \end{pmatrix}, \quad (\text{A7})$$

where the entries indicate the gradient of source brightness distribution in the y_1 and y_2 directions in the source plane. The entries are evaluated at the potential-grid positions $\mathbf{y}_h = \mathbf{x}_h - \nabla\psi(\mathbf{x}_h)$ (the potential grid can be different from the data grid). In addition, if

$$\mathbf{D}_\psi \delta\psi = \begin{pmatrix} \dots & \dots & \dots & \dots & \dots \\ \dots & \frac{\partial \delta\psi_h}{\partial x_1} & \frac{\partial \delta\psi_h}{\partial x_2} & \dots & \dots \\ \dots & \dots & \dots & \frac{\partial \delta\psi_{h+1}}{\partial x_1} & \frac{\partial \delta\psi_{h+1}}{\partial x_2} & \dots \\ \dots & \dots & \dots & \dots & \dots & \dots \end{pmatrix}. \quad (\text{A8})$$

It is then easy to see that $\delta \mathbf{d} = -\mathbf{D}_s(s_p) \mathbf{D}_\psi \delta\psi$ (not blurred) gives a vector whose entries are given by equation (20). The PSF smearing is simply included by multiplying with the blurring operator \mathbf{B} . The gradients can be evaluated through finite-differencing schemes. Higher-order schemes will ensure continuity in the derivatives of the source brightness distribution and potentials.

APPENDIX B: THE ALGORITHM AND IMPLEMENTATION

By solving equation (12), adding the correction $\delta\psi$ to the previously best potential model and iterating this procedure, both the potential model ψ and source model s should converge to a solution that minimizes the penalty function $G(s, \psi)$. We find the following algorithm works very well, typically converging in <100 iterations

1. $i = 0, s_i = \mathbf{0}, \Delta\psi_i = \mathbf{0}$
 $\psi_0 =$ initial model
2. Determine $D_s(s_i), L_c(\psi_0 + \Delta\psi_i)$
3. Solve $(M_c^T M_c + R)\mathbf{r} = M_c^T \mathbf{d}$
using regularization parameters λ_j
4. Extract s_{i+1} and $\delta\psi$ from \mathbf{r}
 $\Delta\psi_{i+1} = \Delta\psi_i + \delta\psi$
 $i = i + 1$
5. Has $G(s_i, \psi_0 + \Delta\psi_i)$ converged?
Yes : Exit
No : Goto 2.

We have implemented this algorithm in PYTHON, using available packages for solving sparse-matrix equations. The code should be relatively easy to parallelize. There are a number of issues that might be worth considering when implementing the algorithm as follows.

(i) Not all of the lens-plane pixels maps on to the finite source plane, and vice versa. We therefore mask those pixels in the lens (source) plane for which the corresponding positions in the source (lens) plane fall outside their pre-defined grids. We make sure we avoid any boundary issues (e.g. ill-defined gradients at the edge of the grid). Masking is properly accounted for in the number of degrees of freedom. Even though formally correct, because the majority of masked pixels have no significant brightness (i.e. the grids are chosen to capture the image and source brightness distributions),

it has little to no impact on the final result. We do not determine in each iteration which source pixel (and corresponding image pixels) are multiply imaged, to check whether they are overconstrained. Although in principle this is the most proper procedure, regularization ensures that even un- or underconstrained pixels are not overfitted (see Fig. 1).

(ii) A linear gradient or additive constant in the potential has no physical meaning (it has no corresponding convergence). In each iteration, we therefore require the solution of ψ to have $\int \psi \equiv 0$ and $\int \nabla\psi \equiv 0$. This also avoids the source to unnecessarily ‘wander around’ in the source plane. A similar issue is that of the mass-sheet degeneracy: $\psi' \leftrightarrow (1 - \kappa_{\text{sh}})\psi + (1/2\kappa_{\text{sh}}\theta^2)$, where θ is some angular distance to a fiducial centre. Nothing observable, other than the time delays change. The algorithm is, in principle, unable to choose between any of these solutions, which all have the same penalty value. As the mass enclosed within the critical curves is well determined (Kochanek 1991) and the mass sheet gives $\kappa_{\text{sh}} = 0$ for our starting model, the final solution of ψ will contain only a small mass-sheet contribution. By adding non-lensing information about the potential (e.g. stellar kinematics; Koopmans & Treu 2004), the mass-sheet degeneracy can be broken.

(iii) The brightest regions of the source often show the strongest curvature (extrema are by definition far from linear). This poses difficulties in reconstructing the brightest regions of the lensed images, as regularization tries to minimize curvature. However, as the brightest areas also have the highest S/N ratio and are therefore well constrained purely through the χ^2 term in the penalty function, one can downweight the regularization term for the brighter pixels in the source solution, if needed.

This paper has been typeset from a $\text{\TeX}/\text{\LaTeX}$ file prepared by the author.